Chemical Science

RSC Publishing

PERSPECTIVE

View Article Online
View Journal | View Issue

Cite this: *Chem. Sci.*, 2013, **4**, 2724

Charge carrier trapping, recombination and transfer in hematite (α-Fe_2O_3) water splitting photoanodes

Monica Barroso,*[a] Stephanie R. Pendlebury,[b] Alexander J. Cowan[c] and James R. Durrant*[b]

Received 21st February 2013
Accepted 23rd April 2013

DOI: 10.1039/c3sc50496d

www.rsc.org/chemicalscience

Hematite is currently considered one of the most promising materials for the conversion and storage of solar energy *via* the photoelectrolysis of water. Whilst there has been extensive research and much progress in the development of hematite structures with enhanced photoelectrochemical (PEC) activity, relatively limited information has been available until recently concerning the dynamics of photogenerated charge carriers in hematite and their impact upon the efficiency of water photoelectrolysis. In this perspective we present an overview of our recent studies of the dynamics of photoinduced charge carrier processes in hematite, derived primarily from transient absorption spectroscopy of nanostructured photoanodes. The relationship between PEC activity and transient measurements are discussed in terms of a phenomenological model which rationalizes the observations and in particular the impact of external potential bias on the relative rates of charge carrier trapping, recombination and interfacial transfer in hematite photoanodes for water oxidation.

1 Introduction

Increasing demand for sustainable, carbon-free energy generation is motivating the development of solar energy conversion and storage technologies. Photoelectrochemical (PEC) water splitting for solar fuel production offers the possibility of capturing solar photons and storing the corresponding energy directly in the bonds of chemical compounds that can subsequently be used in several applications.[1] Significant research efforts are being focused on developing new photoelectrode materials that efficiently harvest sunlight and catalyze the photoelectrolysis of water into molecular oxygen and hydrogen, with semiconductor metal oxides among the most extensively explored for this purpose.[2–4]

Hematite (α-Fe_2O_3) has long been considered one of the most promising materials for solar water splitting applications. Its bandgap (1.9–2.2 eV)[5,6] allows for light absorption in the visible and consequently a potential usage of up to 40% of the solar spectrum. Moreover, hematite is suitable for photoanode applications because its valence band edge (VBE) position is thermodynamically suitable to drive water oxidation (E° (O_2/H_2O) = 1.23 V) by photogenerated holes.[7,8] Also important from the view point of sustainability are the abundance and environmental inertness of hematite, and its chemical stability, particularly in strong alkaline media. However, there are also significant challenges associated with its application to solar driven water oxidation, including long optical absorption depths in the visible part of the solar spectrum (*ca.* 100 nm at $\lambda = 500$ nm),[9] poor carrier mobilities,[10] and short hole diffusion lengths (2–20 nm).[5,8] These together result in substantial electron–hole recombination losses on timescales ranging from picoseconds to milliseconds,[11,12] particularly for charge carriers generated in the bulk of thick films. Other important factors that contribute significantly to the loss of conversion efficiency in hematite are the thermodynamically unfavorable position of the conduction band edge ($E_{CB} \sim 0.4$ V *vs.* RHE),[7,8] unsuitable for unassisted hydrogen evolution, and the sluggish kinetics of water oxidation at the electrode–electrolyte interface[8,13–15] that results in a high overpotential requirement for oxygen evolution. As a consequence of these limitations, high external electric biases are normally required to drive the water photolysis reaction with significant photocurrents. Even in the presence of such electrical bias, solar to hydrogen (STH) conversion efficiencies for hematite, whilst impressive compared to other oxide photoanode materials, are typically significantly lower[16] than the theoretically estimated maximum of 12.8–16%.[17]

Research on hematite photoanodes for water photolysis was initiated nearly four decades ago.[5,18–25] Recent advances in nanomaterials science and computational chemistry methods, alongside progress in the understanding of other metal oxide semiconductors, particularly TiO_2, has opened the way to new strategies for the development of hematite photoanodes,

[a]*Inorganic Chemistry and Catalysis Group, Debye Institute for Nanomaterials Science, Utrecht University, Universiteitsweg 99, 3584 CG, Utrecht, The Netherlands. E-mail: m.barroso@uu.nl*

[b]*Department of Chemistry, Imperial College London, London SW7 2AZ, UK. E-mail: j.durrant@imperial.ac.uk*

[c]*Stephenson Institute for Renewable Energy, Department of Chemistry, The University of Liverpool, Liverpool L69 7ZD, UK. E-mail: a.j.cowan@liverpool.ac.uk*

reinvigorating interest in this material for water photolysis.[26–33] Nanostructuring has been shown to allow some decoupling of the pathways for light capture and hole collection, as a response to the problems of long light penetration depths and short hole diffusion lengths in α-Fe_2O_3.[31,34,35] The preparation of hematite nanowires,[36,37] nanotubes,[38] nanonets,[34] and dendritic nanocauliflowers[39] are examples of successful attempts to achieve improved light harvesting and charge carrier separation. It has also been shown that the mismatch between the conduction band edge position in hematite and the hydrogen evolution potential can be circumvented by coupling a PV unit (*e.g.* a dye-sensitized solar cell) to the hematite photoelectrode to supply the bias voltage required.[40] Finally, surface treatments of hematite with efficient water oxidation electrocatalysts and other metal oxide layers or junctions have also been extensively investigated.[41–46]

It is increasingly recognized that alongside new material developments, improved knowledge of the intrinsic optoelectronic, catalytic and carrier dynamic characteristics of photoelectrode materials will be important for their technological development. In this context, recent theoretical studies have focused on understanding the electronic and catalytic properties of hematite, investigating the nature of electronic transitions and the factors that influence the interaction between the metal oxide surface and water.[47–51] In parallel, a number of experimental studies,[52–55] including those of our group,[11,56–59] have recently focused on the dynamics of photogenerated charge carriers in hematite and the impact of the material improvement strategies discussed above on the rates of charge separation, recombination and interfacial transfer, building upon the work of earlier studies.[60,61] Using mainly electrochemical impedance spectroscopy (EIS) as source of kinetic information, several groups have investigated the physical–chemical processes involved in the photoelectrochemical response of hematite photoanodes for water photolysis.[41,62–64] At the same time, our group has carried out investigations of these dynamics using a combination of transient absorption spectroscopy (TAS), transient photocurrent (TPC) and PEC measurements,[11,56–59] which have allowed us to monitor the fates of photoholes and photoelectrons on the timescale of microseconds to seconds, particularly relevant to understanding the efficiency of the water oxidation mechanism.

This perspective will present an overview of the recent developments achieved in our group and our current understanding of the main factors limiting the efficiency of water photo-oxidation in hematite, specifically by addressing the role of an external electrical bias in the rates of electron–hole recombination, trapping and interfacial charge transfer to the electrolyte in hematite photoanodes.

2 Charge carrier dynamics

2.1 Transient absorption spectroscopy of hematite

Excitation of hematite with visible light of energy higher than the bandgap (λ < 620 nm) leads to the formation of electron–hole pairs. TAS can be employed to characterize the dynamics of these photoinduced charge carriers. Typically, this pump–probe method is based upon the excitation of valence band electrons with a pulsed laser source; the dynamics of the transient species formed – valence band holes and conduction band electrons – can be followed by probing their transient absorption in the visible to near infrared regions of the spectrum using a second probe pulse or beam.

Most previous reports of transient absorption spectroscopy of hematite have focused on ultrafast timescales, and typically reported very fast (<75–150 ps) decay kinetics assigned to the recombination dynamics of photoinduced electrons and holes. Such studies have reported only a very small percentage of charge carriers remaining a few hundreds of nanoseconds after laser excitation.[12,52,54,55,65,66] As such, ultrafast recombination is usually reported as the main fate of the photogenerated charge carriers in hematite, as the short-lived charge carriers are unlikely to have sufficient time to drive the challenging chemistry of water oxidation. It should however be noted that those ultrafast studies are typically carried out with rather high excitation densities, resulting in high photoinduced charge carrier densities, and therefore fast bimolecular (non-geminate) recombination. As a consequence, it is unclear to what extent such ultrafast recombination dynamics impact upon the function of hematite photoanodes under continuous solar irradiation.

Our transient absorption studies on hematite, typically employing rather lower excitation densities, have focused upon the detection of photogenerated charge carriers in the microsecond to second time window. As we discuss below, and indicated by photoelectrochemical analyses, this timescale appears to be highly relevant to photoelectrochemical water oxidation. Fig. 1 shows a typical decay trace obtained upon pulsed laser excitation with UV photons (355 nm, 3.5 eV) of a Si-doped nanostructured hematite film deposited on FTO glass, immersed in an alkaline electrolyte solution and not connected to an external electrical circuit.[11] The transients formed under

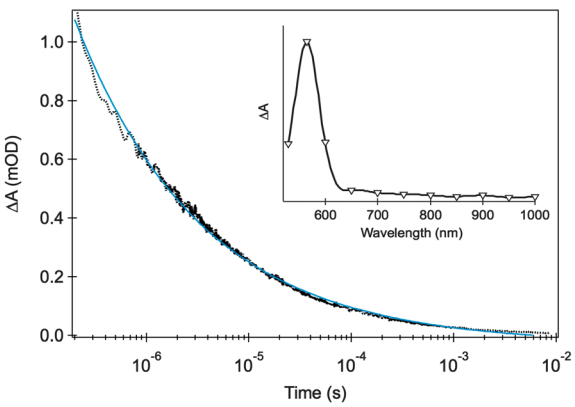

Fig. 1 Transient absorption decay signal for an unbiased Si-doped APCVD α-Fe_2O_3 film upon UV light excitation (355 nm, 200 μJ cm^{-2}, 1 Hz) probed at 580 nm. The inset shows the wavelength dependence of the transient absorption for the same film measured at 500 ns after the excitation pulse. The measurements were performed with the hematite film under Ar, with illumination from the electrolyte/electrode side (front-side or EE illumination). The blue line shows the fit of the transient data with a power law function. Adapted from ref. 11.

such conditions show highly dispersive, power law decay kinetics on the microsecond timescale. Such power law decay dynamics are typically understood as resulting from non-geminate electron–hole recombination that proceeds *via* multiple trapping and detrapping steps, characteristic of semiconductor materials with a high density of trap states,[67] as expected for hematite. The inset in Fig. 1 shows a typical transient absorption spectrum of hematite, measured 500 ns after laser excitation. This spectrum is characterized by a strong absorption band with a maximum at 580 nm and a tail that extends into the near-IR, both features disappearing within a few milliseconds.

The decay dynamics of the photoinduced absorption features shown in Fig. 1 were found to be insensitive to the presence of hole scavengers such as MeOH and KI. This result contrasts with that observed for other metal oxides, particularly with nanocrystalline TiO_2 films, where the presence of chemical electron or hole scavengers typically results in the acceleration of electron or hole decays, respectively.[68] This suggests that the observed micro- to milli-second decay should be assigned primarily to bulk electron–hole recombination.

The intrinsic short carrier lifetimes measured for hematite colloids, single crystals and thin films are often used to justify poor water splitting conversion efficiencies. However, studies of the corresponding charge carrier dynamics under photoelectrochemical water splitting conditions, that is, when the electrodes are integrated in a photoelectrochemical cell and subjected to an external electrical bias, are relatively limited to date.[12] Our own such studies have focused on the bias dependence of transient absorption dynamics on slower microsecond to second timescales. On these timescales, a strong dependence on electrical bias is observed, which we have been able to correlate with the bias dependence of photocurrent.[58]

Fig. 2 summarizes the evolution of the transient absorption spectra of a typical nanostructured hematite photoanode as a function of the applied bias and the time elapsed after laser excitation. Close to the flatband potential (Fig. 2a), the transient absorption spectra resemble that of the unbiased film, showing a transient absorption band that peaks at 580 nm and extends into the near IR. This transient absorption profile disappears in less than a few milliseconds, as seen previously, due to fast trap-mediated electron–hole recombination. As the external bias is made more positive (Fig. 2b–e), it is clear that the transient lifetime is gradually increased by up to three orders of magnitude throughout the spectral window examined. Two distinctive spectral trends can be easily identified: (1) a broad, long-lived transient absorption band (from 550 to >900 nm, with a maximum at 650 nm) forms at sufficiently high positive bias; (2) a relatively narrow, negative transient absorption (bleach) band centered at 580 nm at early timescales gradually develops, from potentials just slightly positive of the flatband potential, increasing as the bias is made more anodic.

Transient decays monitored at 650 nm (Fig. 3a) show a clear biphasic decay. At early times (<10 ms) a relatively fast decay phase is observed, assigned to electron–hole recombination. The kinetics of this recombination are retarded as the anodic bias is increased, assigned to a reduction in the background electron density in the hematite and the concomitant development of a space charge layer.[58] In addition, above a threshold potential of $\sim$0.8 V_{RHE}, a slower decay phase (lifetime $\sim$ 1 s) is also observed, indicating the generation of a residual population of long lived charge carriers (holes, see Section 2.2 below). In contrast, transient decays monitored at 580 nm (Fig. 3b) show a more complex behavior, as we discuss further below (Section 2.3).

2.2 Hole dynamics and water oxidation

The long-lived, broad photoinduced absorption feature peaking at 650 nm is only observed under positive applied voltages, corresponding to conditions where the external circuit will extract photogenerated electrons from hematite film. It is thus reasonable to assign this transient signal to photogenerated hematite holes. The likely physical origin of this 650 nm

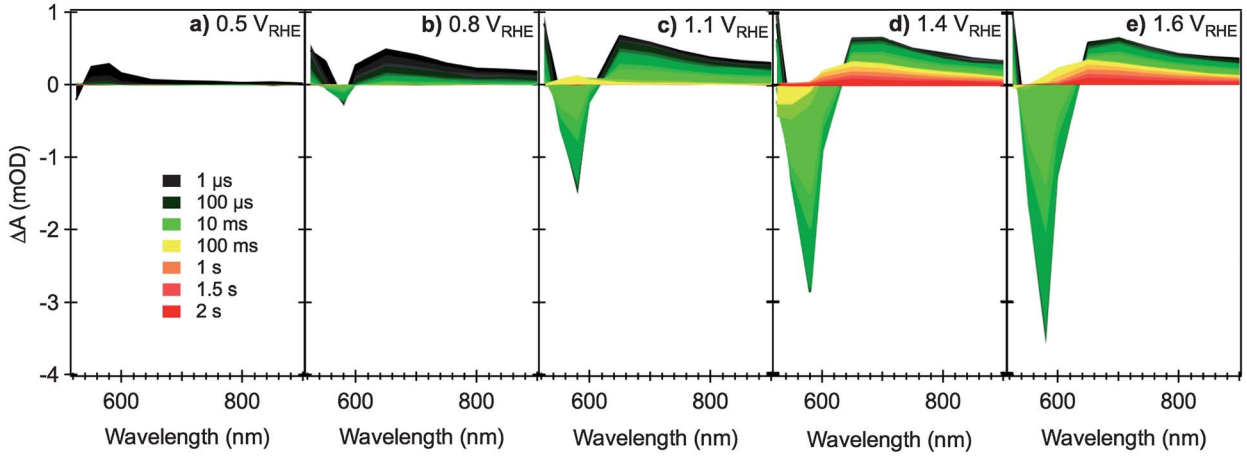

Fig. 2 Transient absorption spectra of nanostructured Si-doped CVD hematite photoanodes under different applied electrical bias as indicated in figures (a) to (e), relative to RHE, in 0.1 M NaOH. The measurements are performed in a three-electrode cell, with Pt gauze as counter electrode and Ag/AgCl/0.3 M NaCl as reference. The nanostructure photoanodes are excited from the electrolyte/electrode side (EE illumination) with a UV laser pulse (355 nm, 200 µJ cm^{-2}, 0.33 Hz) and monitored with the output of a monochromated Xe lamp (75 W). The color code for the spectra time delays is shown in (a). Adapted from ref. 59.

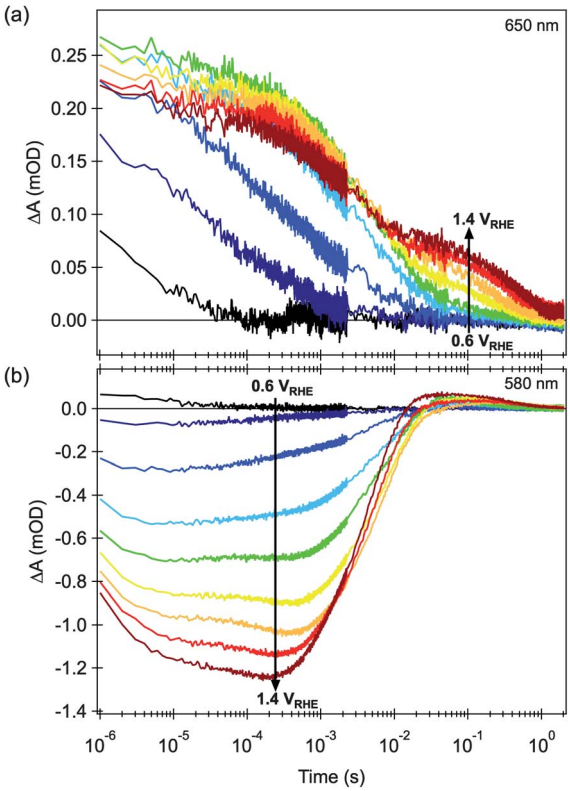

Fig. 3 Effect of applied electrical bias in the transient absorption decay dynamics of nanostructured hematite photoanodes, after bandgap excitation with 355 nm laser light. (a) Probed at 650 nm, and (b) probed at 580 nm. The transient decays shown are measured at 0.1 V intervals within the 0.6 to 1.4 V *vs.* RHE range, as indicated in the figures. Adapted from ref. 58.

absorption is illustrated in Scheme 1 (see Section 5 for more discussion).† In the presence of methanol, a well-known hole scavenger, the lifetime of this slow decay phase is reduced ~5 fold, confirming its assignment to holes and indicating that the decay of this photoinduced absorption is primarily determined by interfacial hole transfer and consequent oxidation of the electrolyte.[11] The effect of bias on the transient absorption shown in Fig. 3a can then be interpreted as follows. Due to the external potentiostatic control, anodic of the flatband, traps and intraband states initially filled with electrons are gradually emptied. As the background density of electrons in the film is lowered a depletion region is formed close to the electrode surface and charge separation is facilitated. As a consequence, electron–hole recombination is gradually retarded, the competition with hole transport is diminished and the photogenerated holes accumulate near the surface, giving rise to the broad long-lived photohole absorption band. More importantly, the lifetime of these holes is potentially long enough (>1 s) to promote the oxidation of water.

Evidence for the assignment of the slow decay phase observed in water electrolytes under positive bias to water

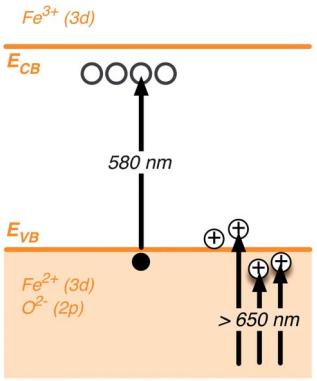

Scheme 1 Schematic illustration depicting the nature of electronic transitions responsible for the Vis-NIR transient absorption spectra of hematite photoanodes.‡

oxidation comes from our observation of a clear correlation between the amplitude of this slow transient absorption decay phase and the PEC performance of hematite. This is shown in Fig. 4a (open circles) revealing a similar threshold potential, and overall bias dependence, for the formation of long-lived photoholes and the observation of anodic photocurrent associated with water oxidation. We have found this correlation is valid for all the hematite photoanodes we have examined so far, regardless of the morphology or doping level,[58] confirming that the formation and possibly accumulation of long-lived photoholes is a prerequisite to the observation of an anodic photocurrent, that is, to the oxidation of water by hematite. Indeed we have observed similar correlations between long-lived photohole yields and photocurrent for nanostructured TiO_2 (ref. 68 and 69) and WO_3 (ref. 70) photoanodes and for hematite photoelectrodes with different surface treatments.[59] As such there appears to be strong evidence in favor of assigning this decay phase to water photo-oxidation, at least under the experimental conditions studied.

Following this assignment of the slow decay phase to water oxidation, it follows that the rate constant for this phase (~1 s^{-1}) corresponds to the rate constant for water oxidation by hematite photoholes. A similar rate constant for this reaction has also been obtained for impedance analyses, supporting this assignment.[62] The yield of these long-lived photoholes is observed to be bias dependent, assigned to the bias dependence of electron–hole recombination. This rate constant was observed to be relatively independent of the type of hematite photoanode studied (nanostructured *versus* flat, doped *etc.*), with measured values ranging from 0.3–3 s^{-1}.

We have measured the temperature dependence of the transient absorption decay dynamics to determine the

† We note Huang *et al.*[12] have reported that hematite conduction band electrons may also show a broad absorption in the red/near IR. This may be the origin of the broad, short lived absorption extending to 1000 nm shown in Fig. 1 inset.

‡ We note the absorption band assigned to hematite holes, peaking at 650 nm, extends as a broad band between 550 and >900 nm. In contrast, the absorption band assigned to optical excitation from the hematite valence band to intraband trap states exhibits a narrow, relatively short lived signal peaking at 580 nm. We note the long lived absorption signal we have reported previously under positive bias at 580 nm (ref. 11) originates from the former broad absorption feature.

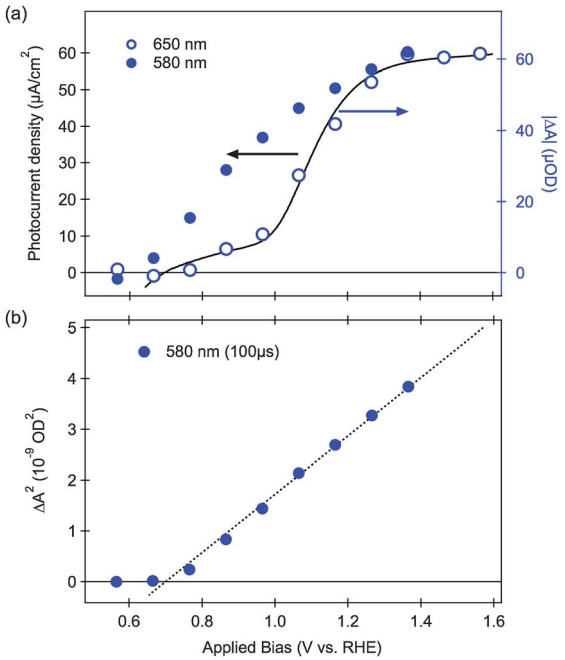

Fig. 4 (a) Correlation between the photocurrent (black line) and absolute transient absorption amplitude (blue circles) as a function of applied electrical bias. Open circles are from transient absorption signals probed at 650 nm at 100 ms after the laser pulse; closed circles are from transient signals probed at 580 nm, 100 μs after the laser pulse. (b) Dependence of the square of the transient bleach (580 nm, 100 μs) with the external electric bias. Adapted from ref. 58.

activation energy for this water oxidation rate constant, found to be 45 kJ mol^{-1}.[57] This significant activation energy at least in part explains the slow timescales of hole transfer to water and confirms slow interfacial kinetics as one of the limiting factors to water oxidation by hematite.[57] Consistent with this analysis, we note that analogous studies of the activation energy for water oxidation by TiO_2 observed no temperature dependence, indicative of significantly smaller activation energy and consistent with the deeper valence band edge for TiO_2 relative to hematite. Consideration of the VBE for hematite and this activation energy relative to the thermodynamics of water oxidation[71] (see Scheme 2) suggests that water oxidation under these conditions proceeds primarily *via* a series of single-hole oxidation steps. We have observed that this rate constant for water oxidation is independent of excitation intensity, at least for the range of laser excitation densities studied,[58] consistent with a one-hole transfer reaction from hematite, possibly to surface adsorbed OH^-, as also suggested by theoretical studies.[72]

The rate constant for water oxidation observed in our studies ($\sim 1\ s^{-1}$) indicates that achieving sufficiently long hole lifetimes is a key requirement for efficient water oxidation. However it should be noted that whilst this timescale is slow relative to electron–hole recombination kinetics, it is actually fast relative to typical turn over frequencies (TOF) reported for most water oxidation electrocatalysts. For example, for the widely studied Co_3O_4 water oxidation catalyst, a TOF $\leq 0.035\ s^{-1}$ per active Co site has been reported.[73] The faster rate constant for water oxidation by hematite holes can most obviously be attributed to the larger thermodynamic driving force for water oxidation by hematite valence band holes (although this is of course at the expense of thermodynamic efficiency). This difference in rate constants might explain, at least in part, a recent controversy over the role of cobalt oxide overlayers in enhancing the water photo-oxidation properties of hematite photoelectrodes.[41,42,56,59,74–76] Our transient absorption studies have shown that thin cobalt oxide overlayers do not result in a significant acceleration of the decay dynamics of hematite photoholes assigned to water oxidation, but rather result in a significant reduction of the electron–hole recombination rate in both unbiased hematite photoelectrodes (Fig. 5) and under applied bias.[56,58,59] We have assigned this reduction of electron–hole recombination losses to the formation of a hematite/cobalt oxide heterojunction that promotes formation of a thicker space charge layer and thus facilitates charge separation. We have suggested that this effect, rather than a catalytic increase in the rate of water oxidation, appears to be the main factor

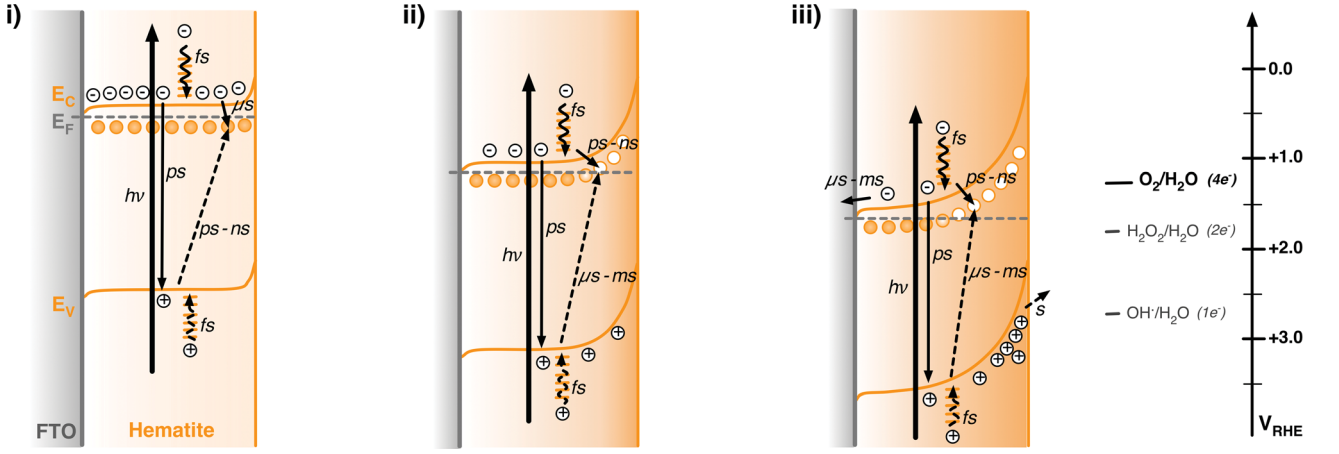

Scheme 2 Schematic illustration of the energy diagrams and processes involving photogenerated charge carriers in n-type hematite photoanodes under illumination and under different external potential biases. (i) +0.5 V_{RHE}, corresponding to the results shown in Fig. 2a; (ii) +1.1 V_{RHE}, for Fig. 2c; (iii) +1.6 V_{RHE}, for Fig. 2e. The relative redox potentials for the one-, two-, and four-electron water oxidation reactions are also shown for comparison with the energy of valence band holes.[71] In the figure, full line arrows represent electron excitation (thick line) and deactivation processes, and dashed arrows represent photohole deactivation processes, following the excitation laser pulse.

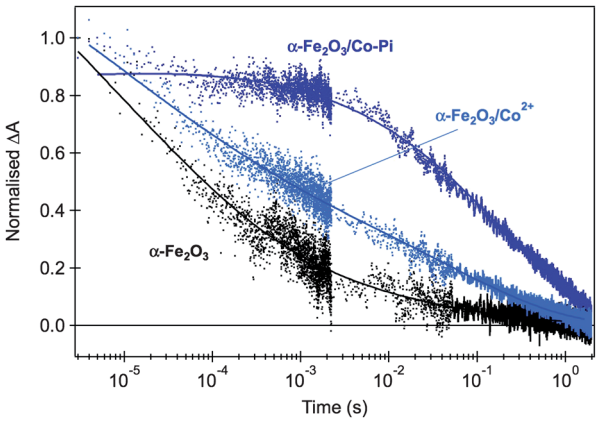

Fig. 5 Normalised transient absorption decays of hematite photoholes probed at 700 nm and obtained with front-side low-intensity UV illumination (355 nm, 200 μJ cm^{-2}) of unbiased APCVD hematite photoanodes, immersed in 0.1 M NaOH aqueous solution. Untreated hematite is shown in black, sample treated by Co^{2+} adsorption is shown in light blue and the composite α-Fe_2O_3/Co-Pi is shown in dark blue. Adapted from ref. 59.

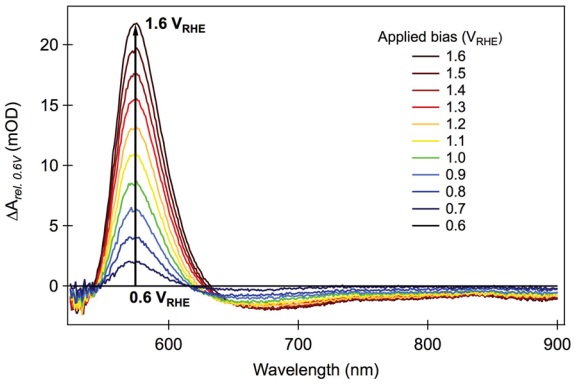

Fig. 6 Difference steady-state absorption spectra of hematite photoelectrode under various applied electrical bias. The values plotted in the figure were obtained by subtracting the absorbance at +0.6 V_{RHE} (close to the flatband potential) from the absorbance at each applied potential, in the same range used for the transient absorption studies. Adapted from ref. 59.

determining the decrease observed in the overpotential for oxygen evolution on hematite. A similar conclusion has also been reached from electrochemical impedance analyses.[41] Other heterostructures have also recently been shown to produce similar results.[45,46] Alongside these observations, both we (for example Fig. 5B in ref. 58) and others[74] have reported significant oxidation of the cobalt oxide overlayer under positive applied bias. This oxidation is observed even in the dark under biases where no water oxidation is observed.[53,56] The slow rate constant for water oxidation by cobalt 'holes' relative to hematite holes provides an explanation for why cobalt oxide oxidation appears not to contribute directly to the water oxidation process, at least for the relatively thin cobalt oxide layers employed in our own studies.

2.3 Electron dynamics and charge carrier trapping

Section 2.2 focused upon photohole dynamics, as monitored by their broad photoinduced absorption signal peaking at ~650 nm. We now consider photoelectron dynamics and in particular the role of charge trapping in intraband trap states. In this regard, the second spectral feature apparent in Fig. 2 and 3, namely the sharp absorption/bleaching signal at 580 nm is of particular interest. As we have reported previously,[59] spectroelectrochemical data provide the clearest indicator of the assignment of this 580 nm spectral feature. Such data, comprising steady-state optical absorption spectrum of a hematite electrode as a function of applied bias is shown in Fig. 6. It is apparent from these data that as the film is biased positive from flatband, this 580 nm spectral feature appears as an increasing ground state optical absorption.[59] Related spectroelectrochemical analyses have previously been employed to determine the flatband potential and charge carrier effective masses in TiO_2 and ZnO,[77,78] where the appearance of a bleaching band near the bandgap energy under accumulation conditions was interpreted as resulting from band filling, also known as the Moss–Burstein effect.[79] The 580 nm transient absorption in hematite is then assigned to an optical transition from the valence band into localized states a few hundred meV below the conduction band, as illustrated in Scheme 1. We note that electrons in the tail of the hematite conduction band are generally reported to be relatively localized,[80] such that these states can function as electron traps. The specific nature of these states is further discussed in Section 5.

Following this assignment, we now turn to the analysis of the transient absorption data measured at 580 nm. A positive increase in the 580 nm absorption feature will correspond to an oxidation of these intraband states (*i.e.* to hole trapping) whilst a bleaching of this absorption will correspond to a reduction (*i.e.* electron trapping). In the absence of applied bias, or under cathodic bias close to flatband potential, these intraband states are largely occupied by electrons and therefore function as hole trapping sites. Under these conditions, photoholes can rapidly become trapped in these sites resulting in the appearance of a positive photoinduced absorption signal at 580 nm, as observed in Fig. 1 (inset) and 2a. This absorption signal subsequently decays as photogenerated electrons recombine with these trapped holes (equivalent to electron trapping in vacant electron trap sites). As such these intraband states function as recombination centres for electron–hole recombination. In contrast, under anodic bias, an increasing proportion of these localized band edge states are oxidised, corresponding to those within the space charge layer. Under these anodic bias conditions, photoexcitation in the space charge layer results in trapping of photogenerated electrons in these intraband states, causing the observation of a transient bleach band centered at 580 nm (*i.e.* loss of ground state absorption) as observed in Fig. 2c–e. The recovery of this bleach signal occurs on the millisecond timescale, assigned at least in part to recombination of hole with these trapped electrons. As such, these intraband states again act as recombination centres. The magnitude of this 580 nm transient bleaching signal increases with the square route of applied voltage (Fig. 4b). This dependence upon applied bias is analogous to the expected dependence of the

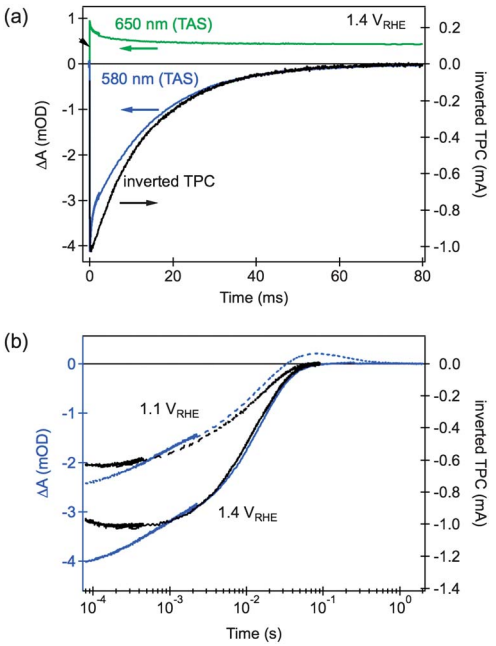

Fig. 7 Comparison of TAS and TPC decays.§ (a) TAS decays probed at 650 nm (green line) and 580 nm (blue), and inverted TPC decay (black), for a hematite electrode biased at 1.4 V_{RHE}; (b) the effect of applied bias on the decay dynamics of the TAS signal probed at 580 nm (blue lines) and inverted TPC (black lines). Adapted from ref. 58.

space charge layer depth W upon applied bias, according to Gärtner's model:[81]

$$W^2 = \frac{2\varepsilon\varepsilon_0}{qN_D}\Delta V_{SC} \quad (1)$$

where ΔV_{SC} represents the potential drop in the space charge layers, N_D the donor density and q, ε and ε_0 are constants representing the electron charge, the dielectric constant and the permittivity of the vacuum, respectively. This similar $V^{1/2}$ dependence suggests the transient bleach signal originates from charge carriers generated within the space charge layer, as illustrated in Scheme 2.

Further confirmation of the assignment of the bleaching feature to trapped electrons is obtained from comparison of the dynamics of transient absorption and transient photocurrent decays, presented in Fig. 7. The transient photocurrent signal is proportional to the rate of charge extraction from a photoelectrode at a given time, from which the charge remaining in the film at a given time can be calculated.[58] The similarity between the kinetics of bleach recovery and transient photocurrent decay, particularly at sub-millisecond timescales, is consistent with the competition between electron–hole recombination and charge collection. Trapped electrons are then expected to either recombine with holes, as probed by the decay of the positive 650 nm transient absorption signal, or be swept out of the space charge layer by the electric field present within this layer and then collected in the external circuit, as measured in the transient photocurrent response.

§ Ideally TAS should be compared with the *charge remaining to be extracted*, but where the TPC kinetics are dominated by electron–hole recombination, as in the present case, both the TPC decay and charge remaining decay will be approximately single exponential.

3 Model for photoelectrode function

Scheme 2 illustrates a simple model of hematite photoelectrode function under pulsed laser excitation based upon the results discussed above. This model includes both conduction band electrons and valence band holes, as well as the intraband states located a few 100 mV below the conduction band edge discussed in Section 2.3. These intraband states can function as either electron or hole traps depending upon their oxidation state, in either case they can mediate electron–hole recombination. The model employs the assignments of the 650 and 580 nm spectral features given in Section 3 to explain the bias dependence of the kinetic data shown in Fig. 1–3. It is presented as a model to describe response of hematite under pulsed laser excitation – the relevance of this model to continuous operation under solar irradiation is discussed in Section 2. We note Scheme 2 includes ultrafast (fs–ns) electron–hole recombination as an additional loss pathway, but this is not considered further in this study.

Under biases close to or cathodic of flatband (Scheme 2(i)), the Fermi level of the photoelectrode is close to the conduction band edge, with the trap states located within the bandgap being largely reduced (*i.e.* occupied by trapped electrons). Following photoexcitation of electrons and holes, a significant fraction of photogenerated valence band holes are rapidly (<1 μs) trapped in these intraband states, resulting in the instrument response limited rise in the 580 nm transient absorption apparent in Fig. 1 and 2a. This photoinduced absorption subsequently decays as photogenerated conduction band electrons recombine with these trapped holes (equivalent to electron trapping into these sites).

Positive (anodic) bias relative to the flatband potential results in partial depletion of electrons from the film, resulting in the formation of a space charge layer at the hematite surface (Scheme 2(ii)). Depending upon the degree of doping and nanostructuring, and the magnitude of the applied bias, this space charge layer can extend up to 10's of nanometers into the hematite film.[58] Under these conditions, intraband states located below the conduction band and within the space charge layer become oxidized (vacant of electrons), resulting in the appearance of the 580 nm ground state absorption apparent in Fig. 6. Upon photoexcitation, conduction band electrons within the space charge layer are rapidly (<1 μs) trapped into these oxidized intraband states, causing the bleaching of this 580 nm absorption signal. This population of trapped electrons subsequently decays on the microsecond – 10 ms timescale *via* two distinct processes. At modest anodic biases, recombination of the trapped electrons with photogenerated holes (Fig. 7) dominates. At significantly anodic biases, an increasing proportion of trapped electrons are swept out by the space charge layer electric field and collected by the external circuit (Scheme 2(iii)). Finally, residual holes that did not recombine with photogenerated electrons accumulate at the

photoelectrode surface and drive the oxidation of water on the seconds timescale. The proportion of holes that avoid electron–hole recombination, and are thus able to accumulate at the hematite surface to drive water oxidation, increases with increasing anodic bias, as illustrated in Scheme 2(iii).

4 Relevance to photoelectrochemical water splitting under continuous illumination

Most models of hematite photoanode function have been developed on the basis of frequency domain electrochemical studies, or photocurrent/photovoltage transients.[7,8,41,62–64,74,82,83] Such analyses are typically undertaken in the presence of continuous irradiation using only a low intensity voltage or optical perturbation, and can therefore be directly related to continuous device operation. However we note that such photoelectrochemical techniques are typically limited to the measurement of electrical output alone (which for n-type materials such as hematite photoanodes corresponds to electron based currents/voltages), and are unable to observe processes occurring faster than the semiconductor electron transport time. For example, in nanostructured hematite photoanodes such as those studied herein, the relatively slow electron collection times (milliseconds, see Fig. 7) prevent observation in impedance studies of the faster electron–hole recombination dynamics apparent for example in Fig. 3. Furthermore, such impedance studies do not directly observe photogenerated hole dynamics, but rather infer their behavior from the observed electron dynamics.

The transient absorption data reviewed in this perspective was collected for photoanodes under electrical bias and pulsed laser excitation, but without continuous white light illumination, as this significantly complicates the transient absorption analysis. Several studies employing photoelectrochemical techniques have emphasized that charge accumulation at the semiconductor surface under solar irradiation may have a significant impact upon kinetic competition between recombination and charge transfer.[41,62,82,84] In particular the relatively slow rate constant for water oxidation by hematite holes is likely to result in significant accumulation of photogenerated holes at the hematite surface under continuous irradiation. Such hole accumulation will have a substantial impact upon space charge layer formation at the semiconductor/water interface, and increase the likelihood of multi-hole rather than single hole–water oxidation processes. Transient optical studies under such conditions are currently ongoing, but are beyond the scope of this perspective.

Despite the experimental limitations detailed in the preceding two paragraphs, there is considerable agreement between the results of different experimental techniques. Consistent with the model shown in Scheme 2, photoelectrochemical studies have shown that electron–hole recombination in the depletion layer of hematite can be observed[64,84] and that the diffusion length for photoholes is negligible relative to the space charge layer depth. These two factors explain the small number of photoholes that reach the interfacial region in the absence of a strong positive bias. Those photoholes that effectively reach the interfacial region have been shown to be efficiently collected by fast one-electron hole scavengers, like $[Fe(CN)_6]^{4-}$ and H_2O_2.[14,15] Several electrochemical studies report sluggish water oxidation kinetics on similar timescales to those observed in our transient absorption studies, with these slow water oxidation kinetics limiting photoanode efficiency.[41,62,82,84] Overall, the observed correlation between the yield of long-lived holes measured in our transient studies as a function of applied bias with the current/voltage response of the photoanode is a strong indicator of the relevance of our transient absorption studies to operating PEC devices.

Despite these agreements, some areas of controversy remain, particularly over the role of charge trapping and surface states. Our own studies, and the model illustrated in Scheme 2, have focused on the impact of intraband trap states lying a few hundred millivolts below conduction band – and therefore functioning primarily as electron trap states (at least within the space charge layer, where these states lie above the electron Fermi level). Such electron trap states have also been emphasized in recent photoelectrochemical study by Le Formal *et al.*[83] In contrast, most impedance analyses have included hole trap states lying above the valence band in equivalent circuit models of photoanode function. According to several authors, surface trapping of holes is a key process in the water oxidation mechanism,[41,64] but others have suggested that the reaction is likely to involve the injection of holes accumulated at the valence band[60] (possibly in the form of high valence Fe states). Our own studies do show evidence of hole trapping, apparent as an transient absorption increase at 580 nm in unbiased or cathodically biased films. However our observation that this transient absorption increase inverts to a bleach signal for voltages only a few hundred millivolts positive of flatband suggests that the intraband states associated with this hole trapping lie only a few hundred meV below the hematite conduction band. Within the space charge layer formed under anodic bias, these states primarily function as electron traps, in agreement with Le Formal *et al.*, mediating electron–hole recombination but not directly involved in the water oxidation process.

5 Electronic transitions in hematite

We end by discussing the possible assignment of the electronic transitions in hematite. To do so, it is instructive to start by discussing the nature of its ground state optical transitions, which has remained a subject of debate until recently. In general, three types of electronic transitions are usually associated with α-Fe_2O_3: (i) ligand field (LF) or d–d transitions associated to Fe^{3+} ions; (ii) O 2p → Fe 3d ligand to metal charge transfer (LMCT); and (iii) the pair excitations associated with two magnetically coupled neighboring Fe^{3+} cations. It has been considered for a long time that the transitions responsible for visible light absorption in hematite are indirect Fe^{3+} d–d while strong direct charge transfer transitions between the O 2p and Fe 3d orbitals occur only for energies higher than 3.2 eV. This assignment would be consistent with the wavelength

dependency of the photochemical response of hematite, based on the hypothesis of the formation of two types of holes.[7,85,86] Recently, however, theoretical and experimental studies have indicated that two ligand-to-metal charge transfer bands (O 2p–Fe 3d) occur in the region 440–800 nm.[86,87] *Ab initio* calculations by Hartree–Fock[88] and density functional methods[89,90] have predicted that the highest occupied orbital has a strong O 2p character and the lowest unoccupied energy states are mostly Fe 3d in nature, while soft X-ray absorption and emission spectroscopy studies shave shown of evidence that the valence band is at least strongly hybridized and mostly O 2p in character.[91,92]

Following this discussion, bandgap photoexcitation of hematite most likely occurs due to a charge transfer processes of the type

$$Fe^{3+} + Fe^{3+} \xrightarrow{h\nu} Fe^{4+}(h^+) + Fe^{2+}(e^-) \quad (2)$$

$$O^{2-} + Fe^{3+} \xrightarrow{h\nu} O^-(h^+) + Fe^{2+}(e^-) \quad (3)$$

We are, at this stage, unable to distinguish between Fe^{4+} (or higher valence Fe states) and O^- photoholes.

Donor states in hematite have been associated to oxygen vacancies (V_O) located below the conduction band.[93] Donor-type oxygen vacancies close to the conduction band are observed in several metal oxides and partly responsible for the intrinsic n-type conductivity exhibited by these materials. The nature of traps in Fe^{3+} doped transition metal oxides and perovskites have also been extensively investigated in the early 1970s.[94] According to Clark and Broadhead, the photochromism in Fe^{3+} doped rutile is associated to hole trapping by ferric acceptors; electrons are trapped at a Fe^{3+}–V_O complex forming a Fe^{2+}–V_O chromophore, and Fe^{4+} is not involved in the induced optical absorption, but only serves as a recombination site for the bleaching process.[95] Conversely, Faughnan and Kiss consider that the electron trap is an oxygen vacancy and the chromophore is the Fe^{4+} ion created by hole trapping.[96] Our results are consistent with Clark and Broadhead's model whereby increased ground state absorption is observed as the states are oxidized. We therefore tentatively assign the localized states responsible for the spectral features observed at 580 nm in our experiments to iron–oxygen vacancy complexes, as summarized in Scheme 1.

6 Conclusions

Transient absorption spectroscopy has previously been shown to be a powerful probe of charge carrier dynamics in photovoltaic devices such as dye sensitised solar cells.[97] In contrast, such studies of photoelectrochemical water splitting systems are relatively underdeveloped. The results we have reviewed herein demonstrate that transient absorption studies can indeed provide key insights into the charge carrier kinetics relevant to water photo-oxidation for one such photoanode, hematite. By monitoring the dynamics of transient decays assigned to hematite photogenerated holes and electrons on timescales of μs to s, we were able to propose a phenomenological model that describes the role of external electrical bias on the photoinduced charge carrier dynamics in this material, in the context of photoelectrochemical water splitting applications. Spectral evidence for the formation of long-lived photoholes under external applied biases positive of the flatband, together with the decrease in the electron–hole recombination rate show the importance of decreasing the background electron-density in hematite photoanodes for efficient water oxidation to occur. Furthermore, our studies highlight the role of applied bias on the trapping of electrons and holes at available intraband states, following light excitation.

These results are shown to provide information complementary to more conventional electrochemical studies such as impedance analyses. As such, these studies yield key insights into the factors determining the efficiency of solar driven fuel synthesis by hematite photoelectrodes. They moreover demonstrate the potential of transient optical studies as a powerful probe of photoelectrochemical function likely to be applicable to other systems addressing the grand challenge of solar fuel generation.

Acknowledgements

Financial support from the Engineering and Physical Sciences Research Council, and the European Research Council (Project Intersolar), is gratefully acknowledged. We thank Dr Piers Barnes and Dr Florian Le Formal for helpful discussions.

Notes and references

1 M. Grätzel, *Nature*, 2001, **414**, 338–344.
2 F. E. Osterloh, *Chem. Mater.*, 2008, **20**, 35–54.
3 A. Kudo and Y. Miseki, *Chem. Soc. Rev.*, 2009, **38**, 253–278.
4 M. G. Walter, E. L. Warren, J. R. McKone, S. W. Boettcher, Q. Mi, E. A. Santori and N. S. Lewis, *Chem. Rev.*, 2010, **110**, 6446–6473.
5 J. H. Kennedy and K. W. Frese, *J. Electrochem. Soc.*, 1978, **125**, 709–714.
6 L. A. Marusak, R. Messier and W. B. White, *J. Phys. Chem. Solids*, 1980, **41**, 981–984.
7 J. H. Kennedy and K. W. Frese, *J. Electrochem. Soc.*, 1978, **125**, 723–726.
8 M. P. Dareedwards, J. B. Goodenough, A. Hamnett and P. R. Trevellick, *J. Chem. Soc., Faraday Trans. 1*, 1983, **79**, 2027–2041.
9 R. F. G. Gardner, F. Sweett and D. W. Tanner, *J. Phys. Chem. Solids*, 1963, **24**, 1183–1196.
10 F. J. Morin, *Phys. Rev.*, 1951, **83**, 1005.
11 S. R. Pendlebury, M. Barroso, A. J. Cowan, K. Sivula, J. W. Tang, M. Grätzel, D. Klug and J. R. Durrant, *Chem. Commun.*, 2011, **47**, 716–718.
12 Z. Q. Huang, Y. J. Lin, X. Xiang, W. Rodriguez-Cordoba, K. J. McDonald, K. S. Hagen, K. S. Choi, B. S. Brunschwig, D. G. Musaev, C. L. Hill, D. W. Wang and T. Q. Lian, *Energy Environ. Sci.*, 2012, **5**, 8923–8926.
13 C. Sanchez, K. D. Sieber and G. A. Somorjai, *J. Electroanal. Chem.*, 1988, **252**, 269–290.

14 H. Dotan, K. Sivula, M. Gratzel, A. Rothschild and S. C. Warren, *Energy Environ. Sci.*, 2011, **4**, 958–964.
15 B. M. Klahr and T. W. Hamann, *J. Phys. Chem. C*, 2011, **115**, 8393–8399.
16 J. Brillet, J. H. Yum, M. Cornuz, T. Hisatomi, R. Solarska, J. Augustynski, M. Graetzel and K. Sivula, *Nat. Photonics*, 2012, **6**, 823–827.
17 A. Murphy, P. Barnes, L. Randeniya, I. Plumb, I. Grey, M. Horne and J. Glasscock, *Int. J. Hydrogen Energy*, 2006, **31**, 1999–2017.
18 K. G. McGregor, M. Calvin and J. W. Otvos, *J. Appl. Phys.*, 1979, **50**, 369–373.
19 S. M. Wilhelm, K. S. Yun, L. W. Ballenger and N. Hackerman, *J. Electrochem. Soc.*, 1979, **126**, 419–424.
20 J. H. Kennedy, R. Shinar and J. P. Ziegler, *J. Electrochem. Soc.*, 1980, **127**, 2307–2309.
21 H. Morisaki, H. Ono, H. Dohkoshi and K. Yazawa, *Jpn. J. Appl. Phys.*, 1980, **19**, L148–L150.
22 M. V. C. Sastri and G. Nagasubramanian, *Int. J. Hydrogen Energy*, 1982, **7**, 873–876.
23 R. Shinar and J. H. Kennedy, *Sol. Energy Mater.*, 1982, **6**, 323–335.
24 N. Giordano, E. Passalacqua, V. Antonucci and J. C. J. Bart, *Int. J. Hydrogen Energy*, 1983, **8**, 763–766.
25 K. Itoh and J. O. Bockris, *J. Appl. Phys.*, 1984, **56**, 874–876.
26 T. Lindgren, L. Vayssieres, H. Wang and S. E. Lindquist, *Chem. Phys. Nanostruct. Semicond.*, 2003, 83–110.
27 E. L. Miller, D. Paluselli, B. Marsen and R. E. Rocheleau, *Thin Solid Films*, 2004, **466**, 307–313.
28 A. Duret and M. Gratzel, *J. Phys. Chem. B*, 2005, **109**, 17184–17191.
29 J. A. Glasscock, P. R. F. Barnes, I. C. Plumb, A. Bendavid and P. J. Martin, *Sol. Hydrogen. Nanotechnol.*, 2006, **6340**, U179–U190.
30 L. Vayssieres, *Sol. Hydrogen. Nanotechnol.*, 2006, **6340**, U191–U200.
31 K. Sivula, F. Le Formal and M. Grätzel, *ChemSusChem*, 2011, **4**, 432–449.
32 M. T. Mayer, Y. Lin, G. Yuan and D. Wang, *Acc. Chem. Res.*, 2013, DOI: 10.1021/ar300302z.
33 C. X. Kronawitter, L. Vayssieres, S. Shen, L. Guo, D. A. Wheeler, J. Z. Zhang, B. R. Antoun and S. S. Mao, *Energy Environ. Sci.*, 2011, **4**, 3889–3899.
34 Y. Lin, S. Zhou, S. W. Sheehan and D. Wang, *J. Am. Chem. Soc.*, 2011, **133**, 2398–2401.
35 D. A. Wheeler, G. Wang, Y. Ling, Y. Li and J. Z. Zhang, *Energy Environ. Sci.*, 2012, **5**, 6682.
36 X. Wen, S. Wang, Y. Ding, Z. L. Wang and S. Yang, *J. Phys. Chem. B*, 2004, **109**, 215–220.
37 Y. Ling, G. Wang, D. A. Wheeler, J. Z. Zhang and Y. Li, *Nano Lett.*, 2011, **11**, 2119–2125.
38 S. K. Mohapatra, S. E. John, S. Banerjee and M. Misra, *Chem. Mater.*, 2009, **21**, 3048–3055.
39 A. Kay, I. Cesar and M. Grätzel, *J. Am. Chem. Soc.*, 2006, **128**, 15714.
40 J. Brillet, M. Cornuz, F. Le Formal, J.-H. Yum, M. Grätzel and K. Sivula, *J. Mater. Res.*, 2010, **25**, 17–24.
41 L. M. Peter, K. G. U. Wijayantha and A. A. Tahir, *Faraday Discuss.*, 2012, **155**, 309.
42 D. K. Zhong, M. Cornuz, K. Sivula, M. Grätzel and D. R. Gamelin, *Energy Environ. Sci.*, 2011, **4**, 1759.
43 K. J. McDonald and K.-S. Choi, *Chem. Mater.*, 2011, **23**, 1686–1693.
44 S. D. Tilley, M. Cornuz, K. Sivula and M. Grätzel, *Angew. Chem., Int. Ed.*, 2010, **49**, 6405–6408.
45 Y. Lin, Y. Xu, M. T. Mayer, Z. I. Simpson, G. McMahon, S. Zhou and D. Wang, *J. Am. Chem. Soc.*, 2012, **134**, 5508–5511.
46 Y. Hou, F. Zuo, A. Dagg and P. Feng, *Angew. Chem., Int. Ed.*, 2013, **52**, 1248–1252.
47 I. V. Chernyshova, M. F. Hochella and A. S. Madden, *Phys. Chem. Chem. Phys.*, 2007, **9**, 1736–1750.
48 S. Yamamoto, T. Kendelewicz, J. T. Newberg, G. Ketteler, D. E. Starr, E. R. Mysak, K. J. Andersson, H. Ogasawara, H. Bluhm, M. Salmeron, G. E. Brown Jr and A. Nilsson, *J. Phys. Chem. C*, 2010, **114**, 2256–2266.
49 P. Liao, M. C. Toroker and E. A. Carter, *Nano Lett.*, 2011, **11**, 1775–1781.
50 P. Liao and E. A. Carter, *J. Phys. Chem. C*, 2011, **115**, 20795–20805.
51 A. Hellman and R. G. S. Pala, *J. Phys. Chem. C*, 2011, **115**, 12901–12907.
52 N. J. Cherepy, D. B. Liston, J. A. Lovejoy, H. M. Deng and J. Z. Zhang, *J. Phys. Chem. B*, 1998, **102**, 770–776.
53 B. S. Zou and V. Volkov, *J. Phys. Chem. Solids*, 2000, **61**, 757–764.
54 L. Fu, Z. Wu, X. Ai, J. Zhang, Y. Nie, S. Xie, G. Yang and B. Zou, *J. Chem. Phys.*, 2004, **120**, 3406–3413.
55 A. G. Joly, J. R. Williams, S. A. Chambers, G. Xiong, W. P. Hess and D. M. Laman, *J. Appl. Phys.*, 2006, **99**, 053521–053526.
56 M. Barroso, A. J. Cowan, S. R. Pendlebury, M. Gratzel, D. R. Klug and J. R. Durrant, *J. Am. Chem. Soc.*, 2011, **133**, 14868–14871.
57 A. J. Cowan, C. J. Barnett, S. R. Pendlebury, M. Barroso, K. Sivula, M. Gratzel, J. R. Durrant and D. R. Klug, *J. Am. Chem. Soc.*, 2011, **133**, 10134–10140.
58 S. R. Pendlebury, A. J. Cowan, M. Barroso, K. Sivula, J. Ye, M. Grätzel, D. R. Klug, J. Tang and J. R. Durrant, *Energy Environ. Sci.*, 2012, **5**, 6304–6312.
59 M. Barroso, C. A. Mesa, S. R. Pendlebury, A. J. Cowan, T. Hisatomi, K. Sivula, M. Grätzel, D. R. Klug and J. R. Durrant, *Proc. Natl. Acad. Sci. U. S. A.*, 2012, **109**, 15640–15645.
60 T. Pajkossy, *J. Electrochem. Soc.*, 1983, **130**, 632–635.
61 P. Mulvaney, V. Swayambunathan, F. Grieser and D. Meisel, *J. Phys. Chem.*, 1988, **92**, 6732–6740.
62 K. G. U. Wijayantha, S. Saremi-Yarahmadi and L. M. Peter, *Phys. Chem. Chem. Phys.*, 2011, **13**, 5264–5270.
63 F. Le Formal, N. Tetreault, M. Cornuz, T. Moehl, M. Grätzel and K. Sivula, *Chem. Sci.*, 2011, **2**, 737–743.
64 B. Klahr, S. Gimenez, F. Fabregat-Santiago, T. Hamann and J. Bisquert, *J. Am. Chem. Soc.*, 2012, **134**, 4294–4302.

65 V. A. Nadtochenko, N. N. Denisov, V. Y. Gak, F. E. Gostev, A. A. Titov, O. M. Sarkisov and V. V. Nikandrov, *Russ. Chem. Bull.*, 2002, **51**, 457–461.
66 Y. P. He, Y. M. Miao, C. R. Li, S. Q. Wang, L. Cao, S. S. Xie, G. Z. Yang, B. S. Zou and C. Burda, *Phys. Rev. B: Condens. Matter Mater. Phys.*, 2005, **71**, 125411.
67 J. Nelson, S. Haque, D. Klug and J. Durrant, *Phys. Rev. B: Condens. Matter Mater. Phys.*, 2001, **63**, 205321–205329.
68 J. W. Tang, J. R. Durrant and D. R. Klug, *J. Am. Chem. Soc.*, 2008, **130**, 13885–13891.
69 A. J. Cowan, J. W. Tang, W. H. Leng, J. R. Durrant and D. R. Klug, *J. Phys. Chem. C*, 2010, **114**, 4208–4214.
70 F. M. Pesci, A. J. Cowan, B. D. Alexander, J. R. Durrant and D. R. Klug, *J. Phys. Chem. Lett.*, 2011, **2**, 1900–1903.
71 A. J. Bard, *J. Am. Chem. Soc.*, 2010, **132**, 7559–7567.
72 P. Liao, J. A. Keith and E. A. Carter, *J. Am. Chem. Soc.*, 2012, **134**, 13296–13309.
73 F. Jiao and H. Frei, *Energy Environ. Sci.*, 2010, **3**, 1018–1027.
74 B. Klahr, S. Gimenez, F. Fabregat-Santiago, J. Bisquert and T. W. Hamann, *J. Am. Chem. Soc.*, 2012, **134**, 16693–16700.
75 D. R. Gamelin, *Nat. Chem.*, 2012, **4**, 965–967.
76 D. K. Zhong and D. R. Gamelin, *J. Am. Chem. Soc.*, 2010, **132**, 4202–4207.
77 G. Redmond, A. O'Keeffe, C. Burgess, C. MacHale and D. Fitzmaurice, *J. Phys. Chem.*, 1993, **97**, 11081–11086.
78 B. Enright and D. Fitzmaurice, *J. Phys. Chem.*, 1996, **100**, 1027–1035.
79 T. S. Moss, *Proc. Phys. Soc., London, Sect. B*, 1954, **67**, 775.
80 N. M. Dimitrijevic, D. Savic, O. I. Micic and A. J. Nozik, *J. Phys. Chem.*, 1984, **88**, 4278–4283.
81 W. W. Gärtner, *Phys. Rev.*, 1959, **116**, 84–87.
82 B. Klahr, S. Gimenez, F. Fabregat-Santiago, J. Bisquert and T. W. Hamann, *Energy Environ. Sci.*, 2012, **5**, 7626–7636.
83 F. Le Formal, K. Sivula and M. Grätzel, *J. Phys. Chem. C*, 2012, **116**, 26707–26720.
84 T. W. Hamann, *Dalton Trans.*, 2012, **41**, 7830–7834.
85 N. C. Debnath and A. B. Anderson, *J. Electrochem. Soc.*, 1982, **129**, 2169–2174.
86 M. Gaudon, N. Pailhe, J. Majimel, A. Wattiaux, J. Abel and A. Demourgues, *J. Solid State Chem.*, 2010, **183**, 2101–2109.
87 N. Pailhe, A. Wattiaux, M. Gaudon and A. Demourgues, *J. Solid State Chem.*, 2008, **181**, 2697–2704.
88 M. Catti, G. Valerio and R. Dovesi, *Phys. Rev. B: Condens. Matter Mater. Phys.*, 1995, **51**, 7441–7450.
89 J. Velev, A. Bandyopadhyay, W. H. Butler and S. Sarker, *Phys. Rev. B: Condens. Matter Mater. Phys.*, 2005, **71**, 205208.
90 W. H. Butler, A. Bandyopadhyay and R. Srinivasan, *J. Appl. Phys.*, 2003, **93**, 7882–7884.
91 Y. Ma, P. D. Johnson, N. Wassdahl, J. Guo, P. Skytt, J. Nordgren, S. D. Kevan, J. E. Rubensson, T. Boske and W. Eberhardt, *Phys. Rev. B: Condens. Matter Mater. Phys.*, 1993, **48**, 2109–2111.
92 C. X. Kronawitter, I. Zegkinoglou, C. Rogero, J. H. Guo, S. S. Mao, F. J. Himpsel and L. Vayssieres, *J. Phys. Chem. C*, 2012, **116**, 22780–22785.
93 K. Kobayashi, G. Okada and J. Kumanotani, *J. Mater. Sci. Lett.*, 1988, **7**, 853–854.
94 A. J. Nozik, *J. Phys. C: Solid State Phys.*, 1972, **5**, 3147.
95 W. Clark and P. Broadhead, *J. Phys. C: Solid State Phys.*, 1970, **3**, 1047.
96 B. W. Faughnan and Z. J. Kiss, *Phys. Rev. Lett.*, 1968, **21**, 1331.
97 A. Listorti, B. O'Regan and J. R. Durrant, *Chem. Mater.*, 2011, **23**, 3381–3399.

